Journal of Tethys: Vol. 2, No. 4, 272–286 *ISSN: 2345–2471 ©2014*

Evidence of the Effect of Metasomatism and Introduction Tourmalinite Veins in the Almabulage complex (NW Iran)

Mahboobeh Jamshidibadr[1]

1- Geology Department, Payam Noor University, 19395-4697, Tehran, I.R of Iran.

* Corresponding Author: m_jamshidi@pnu.ac.ir

Received: 25 March 2014 / Accepted: 20 September 2014 / Published online: 28 September 2014

Abstract

Almabulage complex is located in the north of Asadabad city, northwestern Hamedan province, in Sanandaj-Sirjan structural zone. The complex includes several types of low-grade metamorphosed rocks with various protoliths as well as two intrusion having different chemical compositions of synogranite and gabbro. The synogranite intrusion rock has perthite and granophyric co-growths textures and automorph Titanite, along with veins of tourmalinite around it. Given the chemical composition of tourmaline mineral, presence of tourmalinite in several environments is attributed to the presence of boron-content fluids. In the present article, the relationship existing between chemical composition of minerals and metasomatism in the synogranite rock of Almabulage complex has been studied. Tourmaline minerals in tourmalinite veins have radial accumulation as well as zoning. Chemical composition of tourmaline mineral has been analyzed using the Electron Micro Probe Apparatus, EPMA, at the University Japanese Naruto. Lack of any defect in the position of X, low value of Al, relative frequency of Mg, Ca, and chemical zoning are all indications of formation of tourmalinite veins in hydrothermal environments. Furthermore, presence of sodic minerals and the obvious anomaly of Na in plagioclases, which makes those plagioclases having zoning to be appeared as rich in Albite, as well as formation of metal minerals of magnetite type in this complex all may be considered as evidence of the effect of alkaline metasomatism in Almabulage complex.

Keywords: Tourmaline, Almabulage complex, Synogranite, Hydrothermal fluids.

1–Introduction

Chemical composition of rock-forming minerals as well as of some minor minerals may be practically used in genesis and crystallization of magma. Also, using electron microprobe analyses which are conducted to determine the chemistry of individual minerals, along with field studies, petrography and geochemistry of the whole rock may be practical when interpreting the genesis process of magma. Chemistry of tourmaline (e.g., Henry and Guidotti, 1985; Henry and Dutrow, 1992, 1996; London and Manning, 1995; Trumbull and Chaussidon, 1999; Williamson *et al.*, 2000; Altherr *et al.*, 2004; Marschall *et al.*, 2006), for instance, may be considered as one of the studies that researchers have already carried out on the process of elements distribution in feldspars (Vance, 1965; Wiebe, 1968; Loomis and Welber, 1982; Blundy and shimizu, 1991).

Chemistry of feldspars, which are counted among the main constituents of acidic igneous rocks, process of distribution of elements as well as the exsolutions existing among them, may be also used in interpretation of the formation of igneous.

Tourmaline is often found in form of a minor mineral. Boron is an incompatible element that is present in very low abundance in crust and mantle rocks in form of a fluid (e.g., Ryan and Langmuir, 1995; Taylor and McLennan, 1985). In order to tourmaline formation, 3 weight percent of boron oxide are required. This is mainly in relation to magmatic processes and those fluids which are associated with them. Among the characteristics of tourmaline are complex chemical compositions, usual appearance of zoning, and effect of diffusion and decomposition on partial change in its chemical composition during its growth process (Henry and Guidotti, 1985; Henry and Dutrow, 1992, 1996). Tourmaline may be the main or a minor constituent of a rock as, for example, in tourmalinite (e.g., Slack *et al*., 1984), granites, pegmatites, and tourmaline-content greisens (eg., Trumbull and Chaussidon, 1999), quartz and tourmaline-content granites sections (e.g., London and Manning, 1995; Williamson *et al*., 2000) eclogites and tourmaline-content serpentinites (e.g., Altherr *et al*., 2004; Marschall *et al*., 2006).

In this article, mineral chemistry of feldspar and tourmaline, metallic minerals in combination with the results obtained from systematic field studies, petrography, and geochemistry has been discussed and investigated so as to determine the trend of crystallization of synogranite intrusion in Almabulage complex.

2- Materials and Methods

2-1. General Geology of Almabulage Complex (AC)

Almabulage complex is located in 15 kilometers to the northwestern of Hamedan, outcropped in Northwest Iran, at longitudes 34° 00' to 34° 12' east and latitudes 34° 48' 30'' to 34° 58' north. In terms of structural shape, it has an outcrop in Sanandaj-Sirjan metamorphic zone. AC has been introduced in the 1/100000 geological map of Tuyserkan (Fig. 1).

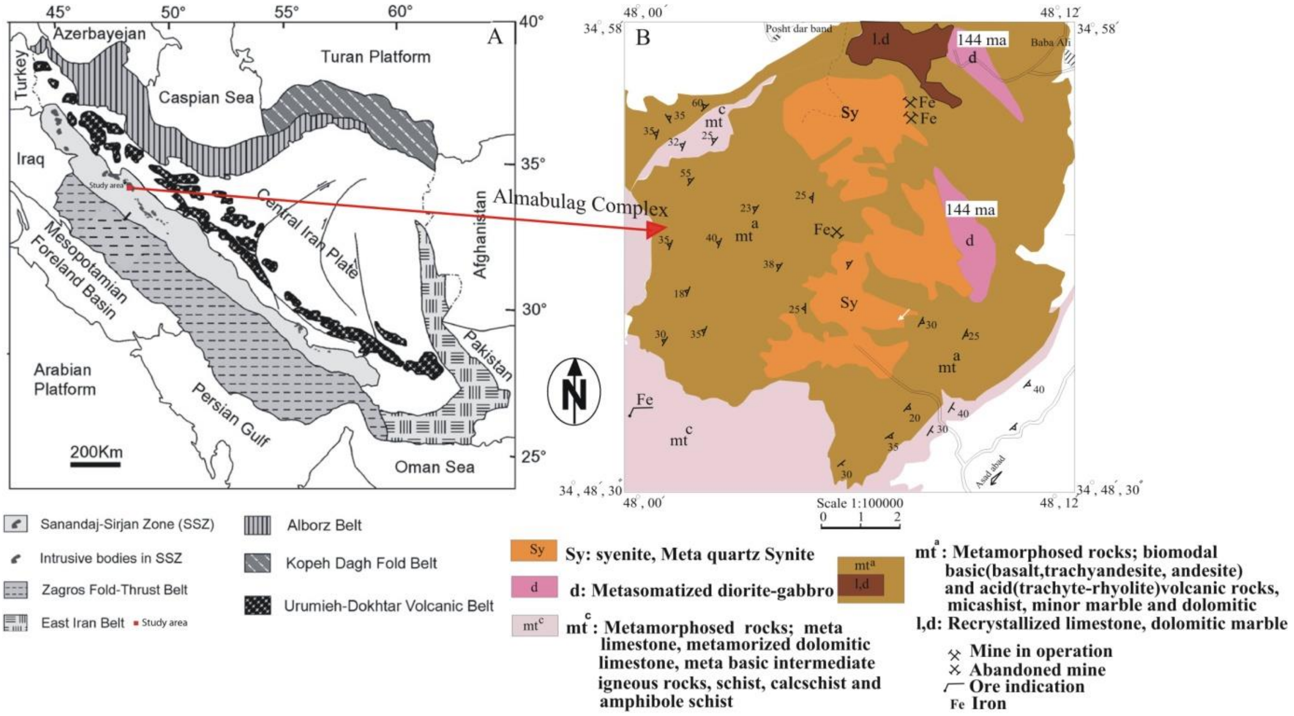

Figure 1A) The Almabulage complex presentation in geological map of Iran from (Ruttner and Stocklin., 1967; Alavi, 1991) with an intrusion and volcanic rocks in Sanandaj-Sirjan zone, Urmia-Dokhtar. B) Simplified geological map of the area from the Tuyserkan 1/100000 geological map (Ashragi and Mahmoudi Garaii, 2003).

It consists of several types of sedimentary units metamorphosed in greenschist facies, as well as two types of igneous intrusive including felsic and mafic igneous rocks. In map of Tuyserkan, the oldest sedimentary units are around Almabulage Mountain that is a sedimentary-volcanic series which has been metamorphosed in the greenschist facies. It includes meta-rhyodacite, metarhyolite, and dolomitic limestone and marble rocks with white, green, and light gray colors. These rocks have been highly metasomatized and metamorphosed, having outcrop in green color. There is also a set of outcrops in AC consisting of sedimentary units named Chenarsheikh, which include lime and dolomitic rocks with light gray color, banded texture and sugar grain-like texture. Its lithological composition includes limestone, marble and dolomitic marbles, along with phyllite and schist, amphibolite schist and metamorphic sandstones (Figs. 2A and C).

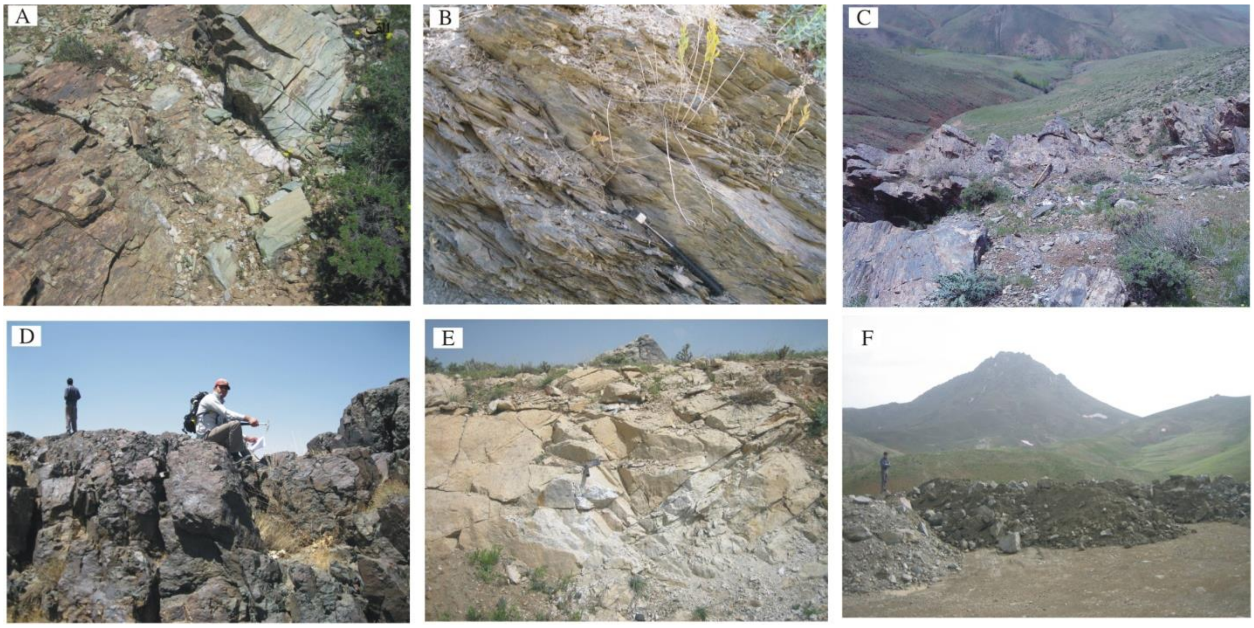

Figure 2) Outcrop different rock units in the Almabulage complex, A) Marbled white and gray in color and limestone, B) Schists show a distinct schistosity, C) Dolomitic limestone with phyllite, D) Mafic intrusion in the North West area near the Baba Ali mine. E) Felsic intrusion in the center of Almabulage complex, E) A felsic intrusion with dome shape in the center of Almabulage complex.

Mafic igneous rocks of AC: this unit named Almabulage metadiorite – gabbro intrusive has outcrops in three points in AC. Its spread is much smaller than the gabbroic intrusion of Sanandaj - Sirjan zone like Hamadan gabbroic intrusion (Fig. 2D). It is gray sometimes having green and dark spots, along with granular texture. The main part of this intrusive consists of plagioclases which have been highly altered and metasomatized. The intrusive has the same metamorphism degree as greenschist facies. Using Rb-Sr method, age of the mafic intrusive has been estimated about 144±7 million years (Late Jurassic-Early Cretaceous) (Valizadeh and Cantagrel, 1975).

Felsic igneous rocks of AC: felsic igneous rocks have outcrops with light gray colour in the middle of AC. They have a smooth, dome-like topography, and most of its area is covered with debris (Figs. 2E and F). The mineralogy of this intrusive has a high percentage of alkali feldspar, but its frequency value is a bit variable in its different parts. The texture is mainly of granular and semi porphyry type which indicates a change in the location of crystallization making crystallization depth happens in shallow depth. Due to the presence of enclaves of the basic intrusion, which are 144 million years old, within the intrusive, age of the felsic igneous rocks with the evidence noted above has been calculated after Jurassic (Valizadeh and Cantagrel., 1975).

Tectonics of Almabulage Complex: Mohajjal and Izadikian (2007) and Jamshidibadr (2013) have introduced four structural deformation stages in AC, including three ductile deformation and a brittle deformation stages as follows:

The first deformation stage: creation of the first generation of folds and foliation;

The second deformation stage: creation of the second generation of folds which have lying to inclined pivot surface and the general trend from Northwest - Southeast (in parallel with the general trend of Sanandaj – Sirjan zone);

The third deformation stage: the third generation of folds, which have vertical axis surface and horizontal pivot with flexural-sliding mechanism. The outcrops related to this stage can be seen in three kilometers from the northwest of Chenar village, near the iron mine. There is also a brittle deformation stage which, in form of a brittle tectonic event, has built some faults in the region. The related outcrop can be seen in five kilometers to the west of Babaali village near to the summit of Almabulage Mountain.

2-2. Economic Ores of AC:

Economic Ores of AC: Babaali iron ore, as an economic mass within AC, has outcrop on the hillside of Almabulage Mountain. Paragenesis of the ore deposit consists mainly of magnetite, pyrite and hematite, along with minor amounts of copper minerals such as chalcopyrite, bornite and malachite. Its gangue minerals include epidote, actinolite, chlorite, quartz, feldspars and calcite. In the sequence of volcanic sediments, the mineral mass is seen as centralized in the central part of the intrusive zone in the shear faces. As one approaches the mineral mass and in rate of alteration increases, the amount of iron is increased (Mohajjel and Izadi kian., 2007; Tavakoli., 2004). Formation of Babaali iron ore has been considered as being done in four stages: the first stage is formation of iron content formations, along with the volcano-sedimentary sequence in the Permo-Triassic rift basin; the second stage includes folding, metamorphism and deformation of the units existing at the same rate as greenschist to Amphibolite facies in Triassic and late Jurassic. In this stage, foliation has been created along the pivot surface of the fold. The stage is along with mobilization of iron centralized towards the direction of the foliation. The third stage is injection of acidic intrusive in an intermediate amount into the iron content units existing in the region and formation of contact metamorphism and skarn-type mineralization in the area in the mid-Cretaceous. The fourth stage is formation of shapeable shear zones in the region along the foliation (caused by intrusive rock) simultaneous with the residual phases of the intrusive rocks, and migration of the iron ores and their centralization in the shear zones.

2-3. Sampling

Sampling has been done in a systematic way in Almabulage complex. Considering the active tectonic of the region and effect of the metamorphism phases, in the synogranite intrusive, which is the main subject of the present article, in particular and during the sampling process for preparing sections and conducting analyses, it has been tried to make the sampling process to be done on those rocks which have no sign of weathering.

2-4. Analytical methods

Using a 15 KV acceleration voltage and electricity current of 15 nA, chemical analysis on the minerals has been carried out after preparing smooth sections by the model JXA-8800R (WDS) electron microprobe apparatus in the geological science section of the University of Naruto, Japan. Chemistry of those minerals whose whole rock geochemistry had been analyzed in previous studies (Shafiee *et al*., 2013; Amiri, 1996) was used to be analyzed in the present research. BSC images of zoning in tourmaline mineral and Rim to Rim surface analysis on tourmaline mineral have been conducted by using the SEM apparatus model σvp so as to identify the distribution of elements in it in the center for practical researches of Geological Survey and Mineral Exploration of Iran, Karaj branch.

3- Discussion

Frequency of minerals in the felsic intrusive of AC varies with a small percentage including quartz (20 to 30 percent), plagioclases (20 to 40 percent), and alkali feldspar (40 to 60 percent) whose frequency is higher than that of quartz and plagioclase. Given the frequency of each of the minerals forming the rock, composition of this intrusive varies between alkali feldspar–synogranite and syenite, having synogranite as the most frequent mineral. Because of this, the felsic intrusive of AC is named for synogranite in this article. In the petrography study on the intrusive synogranite, the plagioclases are seen as being shaped to semi-shaped and having a kind of zoning whose center is in form of co-growth of micro antiperthite. Quartz is seen as amorphous generally having lesser size of crystals than plagioclases and alkali feldspars. Alkali feldspar has large crystals with Carlsbad twining pattern and a variety of co-growths in macro-, meso- and stain micro perthite forms having several spot- and string-like states (Figs. 3A, B and C).

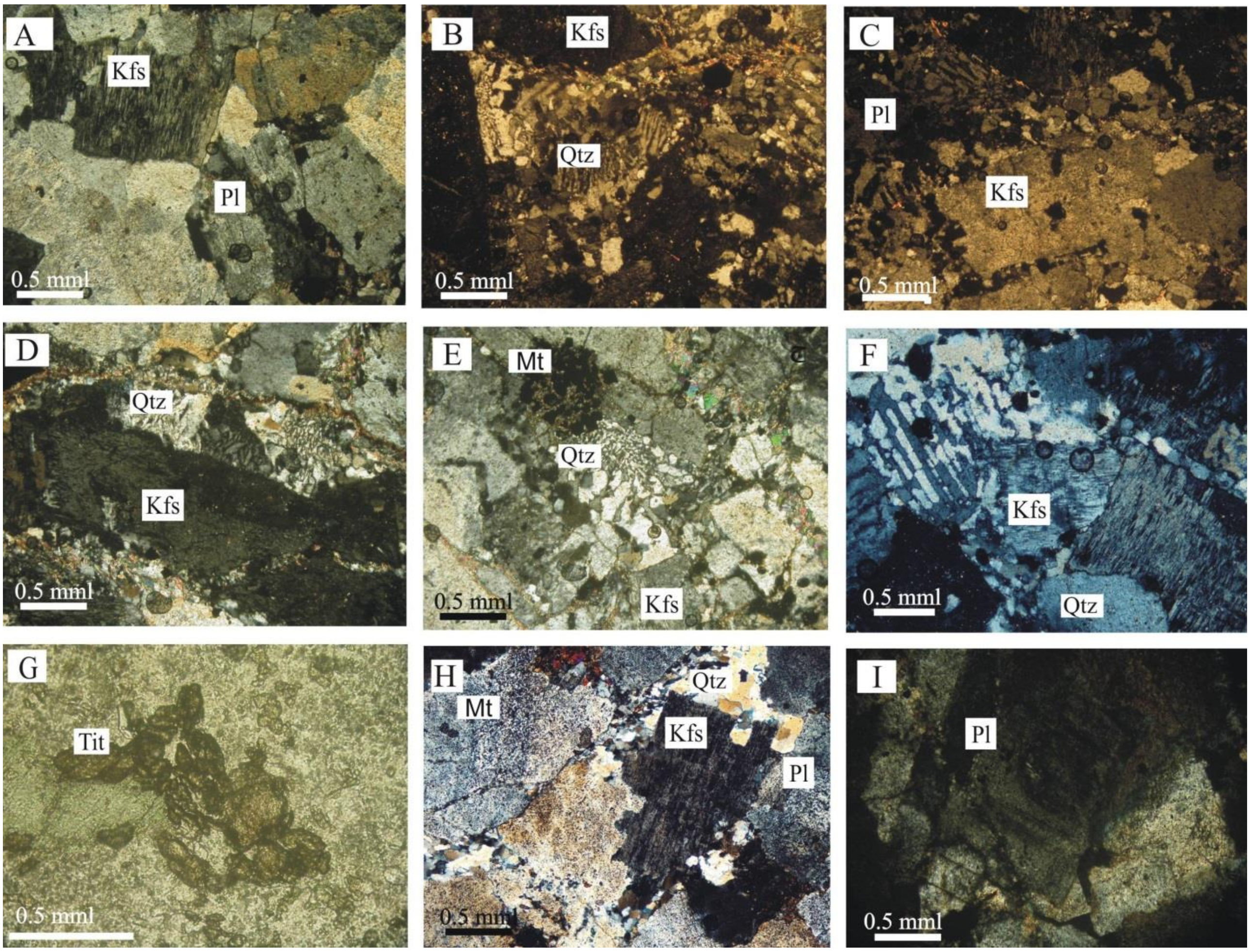

Figure 3) Microphotograph of representative syenogranite samples of Almabulage complex (XPL light). A) Different co-growths perthite and antiperthite, B) Pseudo- porphyritic texture, C) Granophyric texture, D) The mineral alkali feldspar granophyric texture in the center of the image is shown with twining Karlsbad and perthite texture, E) Granophyric texture and euhedral opaque minerals are shown, F) The perthite and granophyric co-growths are shown, G) Titanite with high relief shown in PPl light, H) Opaque mineral inclusions in plagioclase and alkali feldspar can be seen. I) zoning is in plagioclase. (Pl: plagioclase, Kfs: alkali feldspar, Qtz: quartz, Tit: Titanite, Mt: magnetite).

Frequency of co-growth between alkali feldspar and perthite-type albite plagioclase is more than that between alkali feldspar and antiperthite-type albite plagioclase. In alkali feldspar crystals, there is another co-growth with quartz in form of graphic lines creating a granophyric texture (Figs. 3D, E and F). In addition to the perthite, anti-perthite, and granophyric textures existing in the synogranite intrusive of AC, a pesdu-porphyry texture with wholly crystalline background is seen. In this type of samples, feldspars have a perthite texture meaning that their growth happens in magmatic sub-solvus circumstances. Among the minor minerals of this intrusive, the synogranite of AC including shaped Titanite have been transformed into leucoxene due to alteration in some of the samples (Fig. 3G). Metal minerals of magnetite type crystallized between the plagioclase crystals, and even in some samples, on the plagioclase crystals (Fig. 3H).

There are some dark veins about 10 centimeters thick seen around the synogranite intrusive, all of which are formed from tourmaline that is named tourmalinite in this research. Tourmalines are seen in multi-color forms including pale yellowish green to dark green and olive colors. Its crystals are often shaped, and in some cases, semi-shaped having zoning able to be recognized in cross and longitudinal sections. It also, in some parts, has cumulative growth in radial form (Fig. 4).

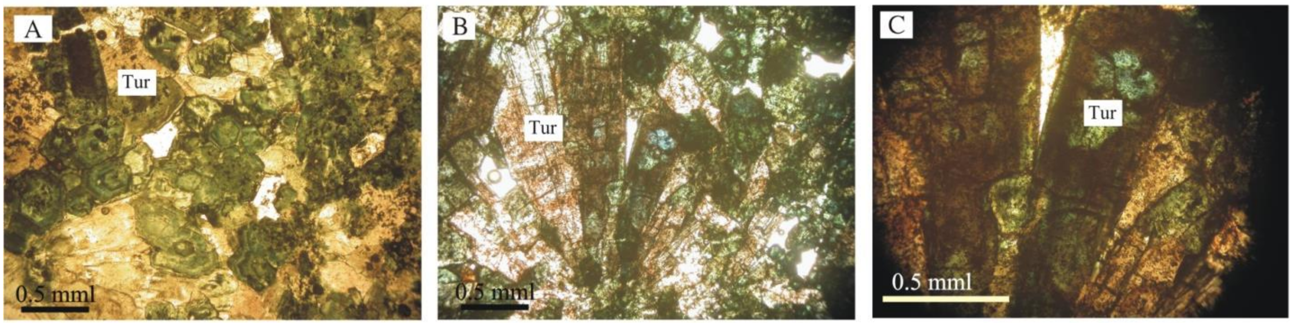

Figure 4) Representative tourmaline minerals in tourmalinitite veins. A) Zoning in tourmaline with green and yellow pleochroism. B and C) Radial accumulation tourmaline crystals, PPl light, (Tur: tourmaline).

3-1. Chemistry of the minerals of AC

Tourmaline: chemical formula of tourmaline mineral is $XY_3Z_6(T_6O_{18})(BO_3)_3V_3W$ (e.g., Hawthorne and Henry, 1999), where X=(Ca, Na, K, vacancy), Y=(Li, Mg, Fe^{2+}, Mn^{2+}, Al, Cr^{3+}, V^{3+}, Fe^{3+}, Ti^{4+}), Z=(Mg, Al, Fe^{3+}, V^{3+}, Cr^{3+}), T=(Si, Al, B), V=(OH, O) and W=(OH, F, O). Frequency of F, B, and Li and the relation $Fe^{3+}/\sum Fe$ cannot be calculated by electron microprobe apparatus. Lack of such a measurement causes a problem in the chemical formula of tourmaline, so a method proposed by some researchers (e.g., Henry and Dutrow, 1996; Clark, 2007) has been used in order to recover the data in tourmalines of the AC. In this method, the whole position of tetrahedron is assumed to be occupied by Si, amount of Fe_{total} divalent iron, and amount of boron three atoms in each formula unit. In other words, normalization has been carried out based on 24.5 atoms of oxygen and the equation T+Z+Y=15. Results of the analysis on the tourmalines of AC have been shown in Tables 1 and 2.

BSC images and SEM analysis on the elements Na, Ca, Mg, and Fe indicate the chemical variation and presence of chemical zoning in tourmaline (Figs. 5, 6). The data obtained from the electron microprobe analysis EPMA and the ternary diagrams of Ca, Na^+(K), X have been used in order to identify the type of the tourmalines existing in AC (Fig. 7A). In this diagram, the AC tourmalines are placed in the category of calcic and alkaline tourmalines indicating the replacement of Ca, Na+(K) for and the lack of any vacant space in the position of X. Also, to study the compositional changes in the ratios of Fe, Mg, Na, and Ca and recognize the type of tourmaline, the binary diagram of Fe/(Fe+Mg) and Na/(Na+Ca) have been used (Fig. 7B).

Table 1) Results of electron microprobe analysis (EPMA) of tourmaline minerals. Symbols used in Table "L" longitudinal and "W" cross-section cutting minerals of tourmaline.

Mineral	Tourmaline											
Sample No	1-3-W			1-7-L							4-5-W	
SiO_2	36.15	35.56	35.27	35.88	35.42	35.82	36.27	37.06	36.71	34.34	35.54	36.04
TiO_2	0.13	0.09	0.04	0.19	0.13	0.07	0.18	0.06	0.09	0.31	0.51	0.32
Al_2O_3	29.47	24.33	28.54	28.98	27.59	28.13	27.57	29.41	31.18	26.51	25.81	28.84
Cr_2O_3	0.03	0.00	0.00	0.00	0.01	0.00	0.04	0.02	0.02	0.10	0.02	0.08
FeO	4.27	10.54	8.77	5.96	8.76	9.16	7.56	8.24	3.85	12.37	9.70	7.71
MnO	0.03	0.01	0.01	0.05	0.00	0.00	0.02	0.06	0.04	0.03	0.00	0.00
MgO	10.10	10.41	8.20	9.50	8.29	7.82	9.21	7.79	8.77	7.78	9.77	8.90
CaO	1.11	3.24	2.58	1.92	1.57	1.15	2.47	1.19	0.90	2.83	2.99	2.42
Na2O	2.39	0.92	1.24	1.96	2.10	2.04	1.39	1.91	2.06	1.26	1.26	1.46
K2O	0.03	0.03	0.04	0.02	0.03	0.02	0.00	0.04	0.00	0.05	0.01	0.01
Total	83.71	85.12	84.68	84.45	83.90	84.20	84.71	85.76	83.63	85.56	85.60	85.78
Oxygen	24.5											
Si	6.00	6.00	6.00	6.00	6.00	6.00	6.00	6.00	6.00	6.00	6.00	6.00
Ti	0.02	0.01	0.01	0.02	0.02	0.01	0.02	0.01	0.01	0.04	0.06	0.04
Al	5.80	4.85	5.70	5.72	5.55	5.62	5.47	5.75	6.13	5.31	5.12	5.66
Cr	0.00	0.00	0.00	0.00	0.00	0.00	0.01	0.00	0.00	0.01	0.00	0.01
Fe^{2+}	0.60	1.49	1.24	0.83	1.25	1.30	1.07	1.14	0.54	1.76	1.37	1.07
Mn	0.01	0.00	0.00	0.01	0.00	0.00	0.00	0.01	0.01	0.01	0.00	0.00
Mg	2.52	2.62	2.07	2.37	2.11	1.98	2.31	1.93	2.18	1.97	2.45	2.21
Ca	0.20	0.59	0.47	0.35	0.29	0.21	0.45	0.21	0.16	0.52	0.54	0.43
Na	0.78	0.30	0.41	0.64	0.70	0.67	0.46	0.62	0.67	0.42	0.41	0.47
K	0.01	0.01	0.01	0.00	0.01	0.00	0.00	0.01	0.00	0.01	0.00	0.00
B	3.00	3.00	3.00	3.00	3.00	3.00	3.00	3.00	3.00	3.00	3.00	3.00
Fe/(Fe+Mg)	0.19	0.36	0.38	0.26	0.37	0.40	0.32	0.37	0.20	0.47	0.36	0.33
Na/(Na+Ca)	0.80	0.34	0.47	0.65	0.71	0.76	0.51	0.74	0.81	0.45	0.43	0.52
Fe/(Fe+Mn)	0.99	1.00	1.00	0.99	1.00	1.00	1.00	0.99	0.99	1.00	1.00	1.00
(T+Z+Y)	15	15	15	15	15	15	15	15	15	15	15	15

Table 2) Results of EPMA analysis of minerals, Tourmaline, Titanite, Magnetite crystalline and Magnetite inclusion in the plagioclase.

Mineral	Tourmaline				Magnetite in Pl			Magnetite				Titanite
Sample No	8-10-L				T-51			T-84				T-84
SiO_2	36.49	35.16	36.26	35.62	1.61	3.61	0.77	0.11	0.06	0.58	0.20	30.13
TiO_2	0.20	0.31	0.36	0.44	1.31	1.32	0.14	0.00	0.00	0.08	0.02	31.60
Al_2O_3	29.34	25.94	26.65	25.09	0.32	0.18	0.14	0.02	0.03	0.04	0.02	1.87
Cr_2O_3	0.01	0.08	0.00	0.00	0.00	0.00	0.01	0.02	0.03	0.00	0.00	0.00
FeO	6.29	11.47	7.96	9.64	86.26	86.53	88.45	92.23	91.89	94.07	92.79	4.86
MnO	0.00	0.00	0.01	0.03	0.09	0.14	0.11	0.00	0.04	0.00	0.13	0.12
MgO	9.52	7.12	10.81	10.22	0.03	0.01	0.02	0.00	0.02	0.00	0.01	0.08
CaO	1.92	4.25	3.54	3.72	1.14	1.02	0.05	0.01	0.00	0.00	0.00	26.47
Na_2O	1.87	1.22	0.91	0.84	0.00	0.00	0.03	0.00	0.01	0.00	0.00	0.01
K_2O	0.02	0.02	0.03	0.00	0.07	0.02	0.77	0.02	0.06	0.01	0.00	0.02
NiO	----	----	----	----	0.02	0.00	0.00	0.00	0.00	0.05	0.10	0.00
Total	85.65	85.58	86.54	85.60	90.86	92.84	89.82	92.40	92.16	94.84	93.28	95.16
Oxygen	**24.5**											
Si	6.00	6.00	6.00	6.00	----	----	----	----	----	----	----	----
Ti	0.02	0.04	0.05	0.06	----	----	----	----	----	----	----	----
Al	5.72	5.30	5.19	4.99	----	----	----	----	----	----	----	----
Cr	0.00	0.01	0.00	0.00	----	----	----	----	----	----	----	----
Fe^{2+}	0.87	1.66	1.10	1.36	----	----	----	----	----	----	----	----
Mn	0.00	0.00	0.00	0.00	----	----	----	----	----	----	----	----
Mg	2.35	1.84	2.67	2.57	----	----	----	----	----	----	----	----
Ca	0.34	0.79	0.63	0.67	----	----	----	----	----	----	----	----
Na	0.60	0.41	0.29	0.28	----	----	----	----	----	----	----	----
K	0.00	0.01	0.01	0.00	----	----	----	----	----	----	----	----
B	3.00	3.00	3.00	3.00	----	----	----	----	----	----	----	----
Fe/(Fe+Mg)	0.27	0.48	0.29	0.35	----	----	----	----	----	----	----	----
Na/(Na+Ca)	0.64	0.34	0.32	0.29	----	----	----	----	----	----	----	----
Fe/(Fe+Mn)	1.00	1.00	1.00	1.00	----	----	----	----	----	----	----	----
(T+Z+Y)	15	15	15	15	----	----	----	----	----	----	----	----

As shown in the diagram, AC tourmalines are plotted in the range of dravite and uvite, with higher concentration of dravite. Amount of changes in Fe/(Fe+Mg) ranges between 0.19 and 0.48, and in Na/(Na+Ca) between 0.29 and 0.81. The changes indicate the relative frequency of Mg as well as the relative changes in Na and Ca, with the higher frequency of Ca.

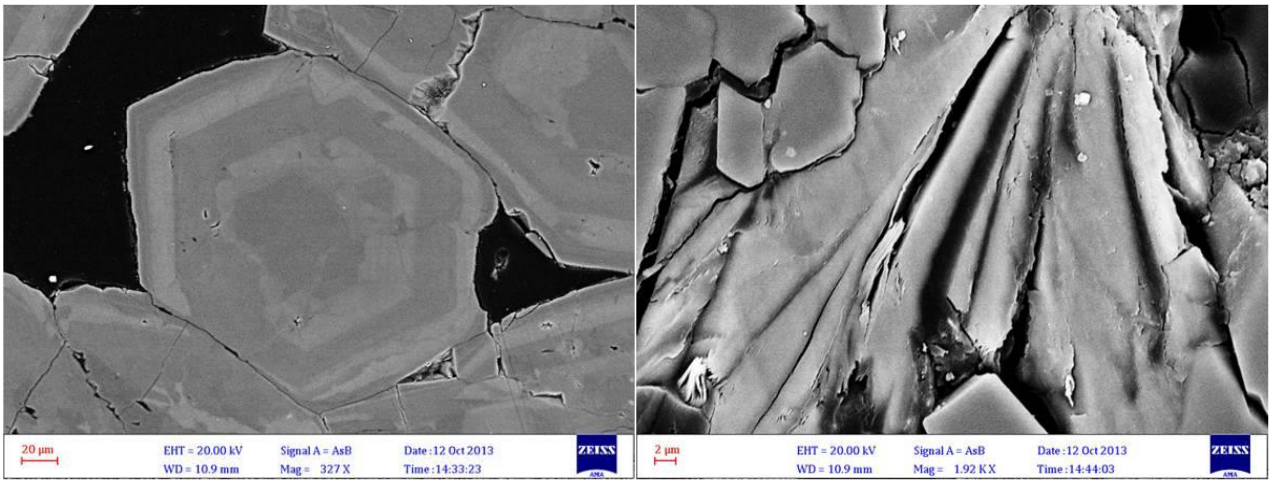

Figure 5) BSC tourmaline Images, A) show cross-section of zoning in tourmaline, B) Radial accumulation tourmaline crystals.

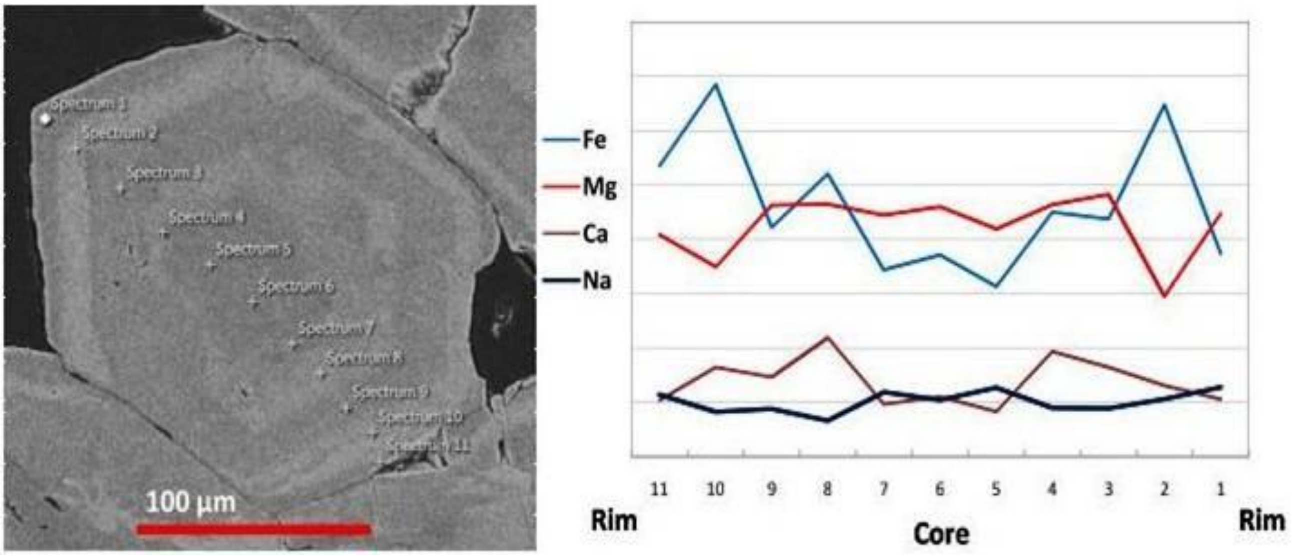

Figure 6A) Rim to Rim SEM analysis for Fe, Mg, Ca, Na elements in tourmaline is shown. B) Cross-section images BSC tourmaline and Show points analyzed Rim to Rim.

Substitutive reactions in tourmaline mineral are carried out in the certain situations of X, Y, and Z. Several diagrams of elements in comparison to the others have been used to study the substitutions (Fig. 7D and F). In the variation diagram of Fe versus Mg, the line Fe/(Fe+Mg)=3 indicates the composition of schorl-dravite and the space under this line shows substitution of Al in the position Y, and the space above the line is an indicator of the exchange component povondravite or ferrischorl with the formula FeAl$_{-1}$ and uvite. The AC tourmalines are located on the schorl-dravite line, within the area of uvite, above the diagram. Formation of the AC tourmalines in the diagram of changes in Na versus Ca is in connection with the components $(CaO)(NaOH))_{-1}$, $(CaMg_2OH)(Na_{-1}Al_{-2})$, and $(CaMg)(NaAl)_{-1}$ (Fig. 7C). In the ternary diagram Al-Fe-Mg, the AC tourmalines are located in the areas 4 and 5, and in the ternary diagram Ca-Fe$_{(total)}$-Mg, they are located in the areas 3 and 4, indicating that the origin of formation of tourmalinite veins is in the sedimentary units around the AC synogranite intrusion (Figs. 8A and B).

Studying the relative changes in the elements in the chemical formula of tourmaline, it may be understood that the AC tourmalines are considered as hydrothermal because of the followings: large amount of Mg, small amount of the ratio Fe/(Fe+Mg) as well as of tourmaline, small amount of Al, and position of the AC tourmaline i.e. in the external part of the vectors within the diagram R_1+R_2 versus R_3, having a recognizable chemical zoning in microscopic and BSC images (Cavarretta and Puxeddu, 1990; London and Manning, 1995; Trumbull and Chaussidon, 1999). Also the clear fluctuations of the elements Na, Ca, Mg, and Fe during the surface analysis of tourmaline mineral indicates the AC tourmalines to be of hydrothermal origin.

Titanite: In order to make sure about the presence of the minor mineral Titanite, about five points of this mineral have been analyzed, as shown in the table 2.

Opaque minerals: Opaque minerals which, after being analyzed, were identified to be in a shaped form within the samples taken from the synogranite intrusion. The opaque mineral samples, which were taken in form of inclusion in plagioclases in the sample T-84 taken from the southwest of Babaali mine, were analyzed as well. Table 2 shows the results obtained from the analysis of the background opaque minerals and the inclusions.

Plagioclases: Plagioclases have been selected to conduct a microprobe analysis on the AC synogranite intrusive. Of the samples existing in this intrusive and taken from two different samples, the sample T-51, which only has perthite texture from the co-growth textures, and the sample T-84, which has both perthite and granophyric co-growth textures, have been selected to be compared in terms of chemical composition. Also, several crystals of each sample have been analyzed. Among the plagioclases, the one which has zoning has been analyzed, but there were no changes seen in the frequency of sodium and calcium (Fig. 3I). Instead, they both have a frequency higher than that of albite so that the frequency of the molar fraction of albite ranges between 0.95 and 1 Classification of plagioclases is shown in Figure 7E.

Alkali feldspar: The alkali feldspar chosen for analysis includes crystals which have perthite and granophyric textures. Results obtained from the analysis indicate the formation of granophyric texture between alkali feldspars and quartz. Crystals having perthite texture have also a high percentage of orthose. Classification of feldspars using the ternary diagram Ab-An-Or (Fig. 7E) is an indication of abundance of the minerals orthose and albite in the AC feldspars.

3-2. Magmatic series and tectonic of AC synogranite intrusive

AC synogranite intrusive is of metaluminous type. Based on Shand index, we have also A/CNK<1.1 and A/NK>1 indicating it as similar to granites of I type. This type of granitoid igneous rock arises from partial melting of the igneous rocks existing in the lower crust or subtraction of a basaltic magma derived from the mantle (Shafiee *et al*., 2013).

In terms of magmatic series, it is of calc-alkaline type, and most of the samples are located in the magmatic arc environment. In addition, some of the samples are located in the intra-continental regions. These are able to be considered as the effect of the continental crust on calc-alkaline magma (Shafiee *et al*., 2013).

Studying REE diagrams for the AC synogranite intrusive shows the enrichment of light rare earth elements LREE as well as depletion of heavy rare earth elements HREE, which itself indicates the subtraction phenomenon (Shafiee *et al*., 2013). Negative anomaly and depletion in the elements Nb, Ti, and P show the effect of subduction fluids on the genesis of the magma, which is generator of the AC synogranite.

Studies carried out on the multi-element diagrams of the region and enrichment by incompatible elements having large ionic lithophile elements (LILE) indicates the interference of the crust in the evolution of the magma of these rocks.

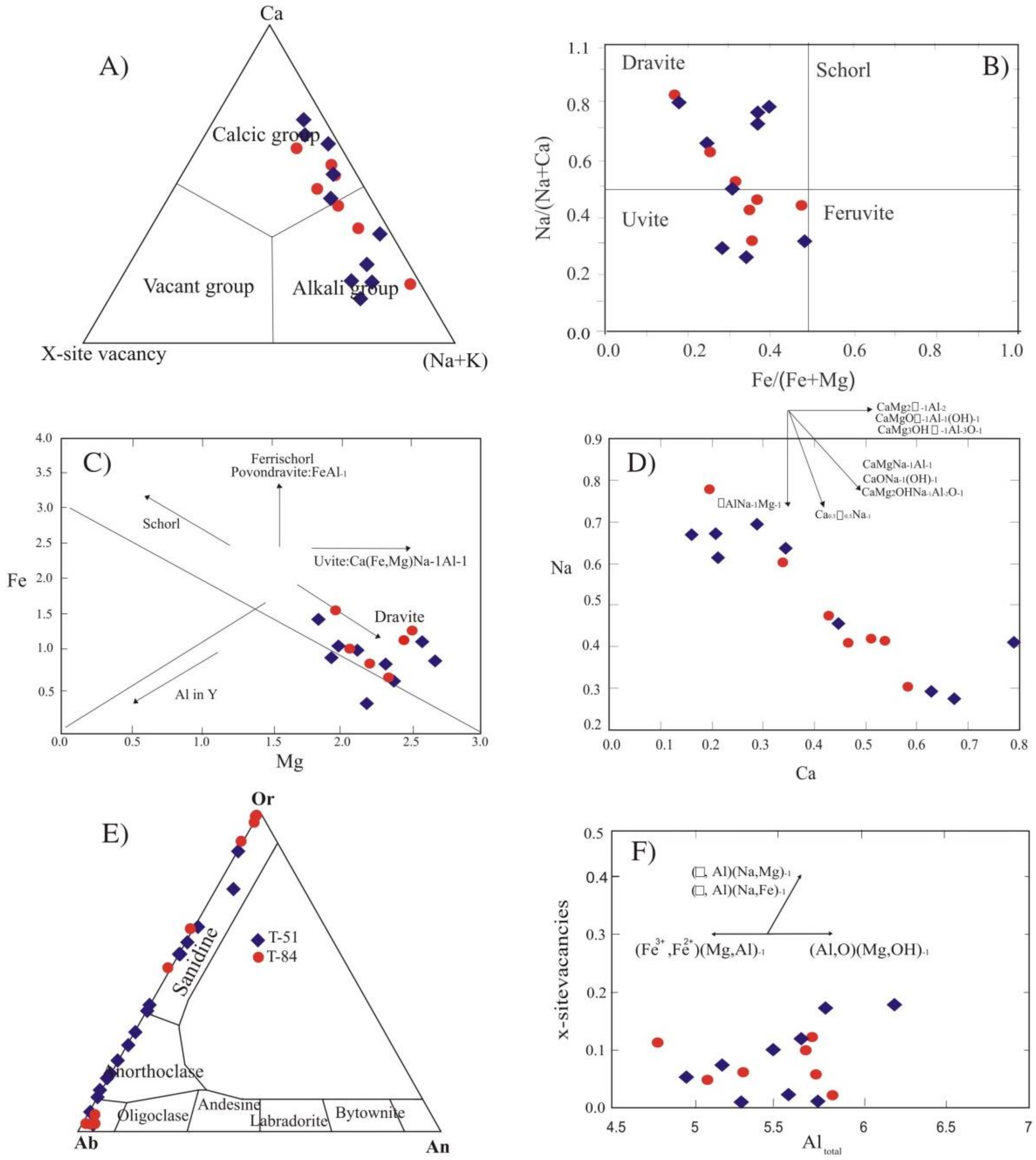

Figure 7) Presentation of AC tourmaline and feldspar in different diagrams. A) Triangular diagram of Ca-X-site vacancy-Na$^+$(K), from (Hawthorne and Henry, 1999). B) Plot of Na/(Na+Ca) versus Fe/(Fe + Mg) from (Trumbull and Chaussidon, 1999). C) Chart Fe relative to Mg, compounds schorl-dravite on line Σ(Fe+Mg)=3 are from (London and Manning, 1995). D) Plot of Na versus Ca, from (Pesquera and Velasco, 1997). E) Ternary diagram Ab-An-Or, F) Plot of the X-site vacancy versus Al$_{total}$ from (Torres-Ruiz et al., 2003). (symbols used in Figures A, B, C, D, F blue rhombic and red circular related to longitudinal and cross-section cutting tourmaline crystals respectively, in Figures D and F shows X-site vacancy).

The negative anomaly of Eu is an indication of subtraction of plagioclase as well as association of the partial crystallization phenomenon (Nagudi *et al*., 2003; Pearce *et al*., 1984).

3-3. Process of replacement and crystallization of AC synogranite intrusive

Given the studies conducted on petrography and chemistry of the minerals forming, the AC synogranite intrusion, in terms of petrography, have got major minerals such as alkali feldspar, plagioclase, quartz and minor minerals such as automorph Titanite and magnetite. According to the geochemical studies, the intrusion have been formed in tectonic environments related to the subduction setting that are of magmatic origin (Shafiee *et al*., 2013). The most important neighboring intrusion is Alvand intrusive, on which new researches and dating have been carried out by Aliani *et al*. (2012). Results show the four separate types of rocks including granite (monzogranite to synogranite), leucogranite (leucotonalite, leucogranodiorite and leucoquartz monzodiorite), mesocratic (tonalite, granodiorite and quartzdiorite) aplitic and pegmatite dyke, with several ages ranging between 147 and 170 million years. From the geochemical point of view, the AC synogranite have more anomalies of alkaline elements than several types of granites separated in the Alvand.

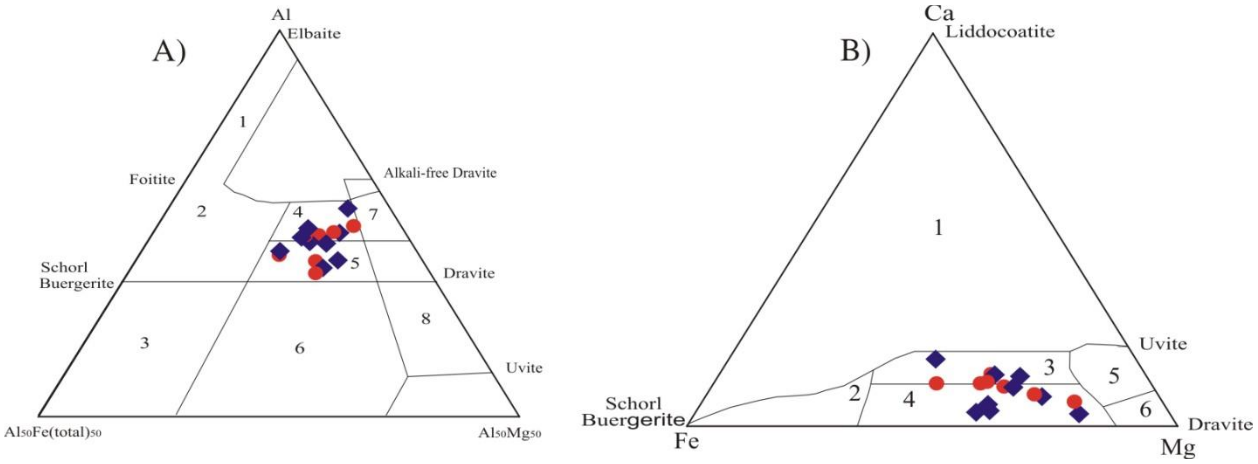

Figure 8A) Al–Fe–Mg diagram for tourmaline from the different farms, with fields after Henry and Guidotti 1985. Labelled fields are: 1) Li-rich granitoid pegmatite and aplites, 2) Lithium-poor granitoids, pegmatites and aplites, 3) Fe^{3+}*-rich quartz–tourmaline rocks (altered granitoids), 4) metapellites and meta-psammites with Al-saturating phases, 5) metapellites and metapsammites lacking Al-saturating phases, 6)* Fe^{3+}*-rich quartz–tourmaline rocks, calc-silicate rocks and meta-pellites, 7) low-Ca meta-ultramafic rocks and Cr–V-rich meta-sediments, and 8) meta-carbonates and meta-pyroxenites. B)* $Ca\text{-}Fe_{(total)}\text{-}Mg$ *diagram from (Henry and Guidotti, 1985). 1) Li-rich granitoid pegmatite and aplites, 2) Lithium-poor granitoids, pegmatites and aplites, 3) rich metapellites Ca, meta-psammites and limestone silica , 4) poor meta-pellites Ca, meta-psammites and rock quartz-tourmaline, 5) meta-carbonate, 6- and meta-ultramafic (signs for tourmaline is used as in Figure 7).*

Based on the studies conducted by some researchers (Johannes *et al*., 1984), those intrusive that have high anomaly of alkaline elements cannot be considered as being in connection with a magmatism stage. AC synogranite intrusive can also be studied and discussed in this regard. The reasons confirming the two replacement stages in the AC synogranite intrusive are presence of pseudo-porphyry and perthite co-growth textures indicating the presence of water vapor with less than 5 kilo bar pressure in the environment, and formation of granophyric textures which happen in form of co-growth on the magmatic cotectic line formed in rapid magmatism cooling circumstances. Considering the active tectonic of the region, Mohajjal and Izadikian (2007) and Jamshidibadr (2013) have introduced four deformation types in connection with formation and replacement of the AC. According to their study, replacement of intrusion is related to tectonic interactions. Formation of the AC synogranite intrusion may be considered as being simultaneous with closing of Neotethys, formed deep beneath the ground, crystallized, and forming perthite and antiperthite co-growth, and at the same time, causing the synogranite intrusion to be located in shallow depth beneath the ground, the region to be dome-like, the cooling process to be done rapidly, and pseudo-porphyry and granophyric textures to be formed, all due to tectonic forces (the second stage of deformation in AC).

High anomaly of alkaline, especially Na, which is confirmed by the chemistry of feldspar minerals, as well as the plagioclases having zoning formed only from albite, all show the effect of hydrothermal fluids on the AC synogranite intrusion and transformation of the intrusion into a sodic one. This transformation and metasomatism in the mafic intrusive, rather than the synogranite intrusion, which is due to the presence of enclaves of the basic intrusion in the synogranite intrusive, has caused the pyroxene existing in the basic intrusion to be replaced by sodic amphiboles, which may be considered as a reason behind the presence of sodic fluids within the environment.

Presence of hydrothermal-type tourmalinite veins and formation of magnetite-type metal minerals has also been introduced as a reason behind the presence and frequency of hydrothermal fluids in several regions of the world such as Willyama Supergroup in Western Australia (Kent and Ashley, 2000).

Some researchers (e.g., Burnham, 1967; Manning, 1981; Pitcher, 1983) believed that fluorine and boron cause increasing in concentration of silica, aluminum, sodium, and potassium in quartz and albite acidic magmatic systems. Of these, increase in concentration of alkalines especially sodium is more than that in aluminum and silica (Glyuk and Anfilogov, 1973; Anfilogov and Glyuk, 1973). The same circumstances happen to the AC intrusive.

4- Conclusion

Almabulage complex felsic intrusion is mainly formed from a series of synogranite rock. It has numerous felsic co-growths between plagioclases and alkali feldspar in different forms including micro-, meso-, and macro-perthite as well as antiperthite textures and a co-growth between alkali feldspar and quartz. Presence of pseudo-porphyry, perthite, and granophyric textures in this intrusion is an indicator of fluctuations existing in the water vapor pressure. Formation of perthite co-growths formed deep beneath the ground with the water vapor pressure of less than 5-kilo bars as well as formation of granophyric and porphyry textures show the rapid cooling of magma in shallow depths. Chemistry of feldspar minerals is also an indicator of the high degree of anomaly of alkaline elements especially sodium, which is seen even at zoning modes of plagioclases. Presence of hydrothermal tourmalinite veins with recognizable chemical zoning and formation of metal minerals in Almabulage complex are also attributed to the relationship between sodic metasomatism and presence of boron- and fluorine-content hydrothermal fluids in the environment.

Acknowledgments:

The author would like to thank Dr. J.Ahmadian for carrying out the some analysis and Dr. K. Ajayebi and Dr. S. Peighambari for their appreciate comments which help us to improve manuscript.

References:

Alavi, M. 1991. Tectonic Map of the Middle East. Geological Survey of Iran, Scale 1: 2900000.

Aliani, F., Maanijou, M., Sabouri, Z., Sepahi, A. A. 2012. Petrology, geochemistry and geotectonic environment of the Alvand Intrusive Complex, Hamedan, Iran. Chemie der Erde – Geochemistry: 72, 363–383.

Altherr, R., Topuz, G., Marschall, H., Zack, T., Ludwig, T. 2004. Evolution of a tourmaline-bearing lawsonite eclogite from Elekdag area (Central Pontides, N Turkey): evidence from for infiltration of slab-derived B-rich fluids during exhumation. Contributions to Mineralogy and Petrology: 148, 409–425.

Amiri, M. 1996. Petrography, petrology and mineral Almabolag area (north of Asadabad), MSc Thesis, Tarbiat Moallem University, Tehran, 186 pages.

Anfilogov, V. N., Glyuk D. S., Trufanova L. G. 1973. Phase relations in interaction between granite and sodium fluoride at water vapour pressure of 1000 kg/cm^2. Geochemistry International: 10, 30–33.

Ashragi, S. A., Mahmoudi Garaii, M. 2003. Tuyserkan geological map, scale 1:100000 Geological Survey and Mineral Exploration country.

Blundy, J. D. Shimizu, N. 1991. Trace element evidence for plagioclase recycling in calc-alkaline magmas. Earth and Plantary Science letters: 102, 178–197.

Burnham, C. W. 1967. Hydrothermal fluids at the magmatic stage, in Barnes, H.L., ed., Geochemistry of hydrothermal ore deposits. New York, Toronto, and London. Holt, Rinehart, and Winston, Inc, pp. 34–76.

Cavarretta, G., Puxeddu M. 1990. Schorl-Dravite- Ferridravite Tourmalines Deposited by Hydrothermal Magmatic Fluids during Early Evolution of the Larderclio Geothermal Field, Italy. Economic Geology: 85, 1236–1251.

Clark, C. M. 2007. Tourmaline: Structural formula calculations. Canadian Mineralogy: 45, 229–237.

Glyuk, D. S., Anfilogov, V. N. 1973. Phase equilibria in the system granite H_2O-HF at a pressure of 1000 kg/cm^2. Geochemistry International: 10, 321–325.

Hawthorne, F. C., Henry, D. J. 1999. Classification of the minerals of the tourmaline group. European Journal of Mineralogy: 11, 201–215.

Henry, D. J., Dutrow, B. L. 1992. Tourmaline in low grade clastic metasedimentary rocks: an example of the petrogenetic potential of tourmaline. Contributions to Mineralogy and Petrology: 112, 203–218.

Henry, D. J., Dutrow, B. L. 1996. Metamorphic tourmaline and its petrologic applications. In boron: Mineralogy, petrology and geochemistry (E.S. Crew and L.M. Anovitz, eda). Reviews in Mineralogy and Geochemistry: 33, 503–557.

Henry, D. J., Guidotti, C. V. 1985. Tourmaline as a petrogenetic metapelites of NW Main. American Mineralogy: 70, 1–15.

Jamshidibadr, M. 2013. The Impact of Different Orogenic Phases on Deformation and Metamorphic of Volcano Sedimentary Rocks in the Almabulage Complex (NW of Iran). Geodynamics Research International Bulletin: 1, 25–37.

Johannes, W. 1984. Beginning of melting in the granite system Qz-Or-Ab-An-H_2O. Contributions to Mineralogy and Petrology: 86, 264–273.

Kent, A. J. R., Ashley, P. M. 2000. Fanning C. M., "Metasomatic alteration associated with regional metamorphism: an example from the Willyama Supergroup, South Australia", Lithos: 54, 33–62.

London, D., Manning, D. A. C. 1995. Chemical variation and significance of tourmaline from southwest England. Economic Geology: 90, 495–519.

Loomis, T. P., Welber, P. W. 1982. Crystallization processes in the Rocky Hill Sanodiorite pluton, California: An interpretation based on compositional zoning of plagioclase. Contributions to Mineralogy and Petrology: 81, 230–239.

Manning, D. A. C. 1981. The effect of fluorine on liquidus phase relationships in the system Qz-Ab-Or with excess water at 1kb. Contributions to Mineralogy and Petrology: 76, 205–215.

Marschall, H. R., Ludwing, T., Altherr, R., Kalt, A., Tonarini, S. 2006. Syros metasomatic tourmaline: evidence for very high-δ^{11} B fluids in subduction zones. Journal of Petrology: 47, 1915–1942.

Mohajjel, M., Izadikian, L. 2007. Poly-deformed Tectonites in Dome Structure of the Almabolagh Region, West of Hamadan. Geosciences (Geological Survey of Iran): 66, 116–133 (In Farsi).

Nagudi, N., Koberl, Ch., Kurat, G. 2003. Petrography and geochemistry of the sigo granite, Uganda and implications for origin. Journal of African Earth Science:, 36, 1–14.

Pearce, J. A., Harris, N. B., Tindle, A. G. 1984. Trace element discrimination diagrams for the tectonic interpretation of granitic rocks. Journal of Petrology: 25, 956–983.

Pesquera, A., Velasco, F. 1997. Mineralogy, geochemistry and geological significance of tourmaline-rich rocks from the Paleozoic Cinco Villas massif (western Pyrenees, Spain). Contributions to Mineralogy and Petrology: 129, 53–74.

Pitcher, W. 1983. Granite type and tectonic environment, Moutain Building processes. London: Academic Press.

Ruttner, A., Stocklin, J. 1967. Geological Map of Iran. Geological Survey of Iran, Scale 1:1000,000.

Ryan, J. G., Langmuir, C. H. 1993. The systematics of boron abundances in young volcanic rocks. Geochimica et Cosmochimica Acta: 57, 1489–1498.

Shafiee, B., Ebrahimi, M., Jamshidibader, M., Maanijoo, M. 2013. The complex Almabolag Co-growth felsic minerals. Twentieth National Conference of Crystallography and Mineralogy of Iran, University of Ahvaz, Iran.

Slack, J. F., Herriman, N., Barnes, R. G., Plimer, I. R. 1984. Stratiform tourmalinites in metamorphic terranes and their geology significance. Geology: 12, 713–716.

Tavakoli, H. 2004. Mineralogy, geochemistry of ore deposits in North West Hamadan, MSc Thesis , University of Madras, 156 pages (in Farsi).

Tavakoli, H., Gaderi, M., Gorbani, M., Mohajjel, M. 2003. New insight on the genesis of iron ore Baba Ali, Hamedan North West. Seventh Symposium of Geological Society of Iran.

Taylor, S. R., McLennan, S. M. 1985. The continental crust: Its composition and evolution. Blacwell, Oxford, U.K.

Torres-Ruiz, J., Pesquera, A., Gil-Crespo, P. P., Vellila, N. 2003. Origin and petrogenetic implications of tourmaline-rich rocks in the Sierra Nevada (Betic Cordillera, southeastern Spain). Cemical Geology: 197, 55–86.

Trumbull, R. B., Chaussidon, M. 1999. Chemical and boron isotopic composition of magmatic and hydrothermal tourmalines from the Sinceni granite-pegmatite system in Swaziland. Chemcal Geology: 153, 125–137.

Valizadeh, M. V., Cantagrel, J. M. 1975. Premières données radiométriques (K-Ar et Rb-Sr) sur les micas du complex emagmatique du mont Alvand, prés d Hamadan (Iran occidental). Comptes Rendus I". Acad. Sci. Paris D 281: 1083–1086.

Vance, J. A. 1965. Zoning in igneous: patchy zoning. Journal of Geology: 73, 636–51.

Wiebe, R. A. 1968. Plagioclase stratigraphy: a record of magmatic conditions and events in a granite stock. American Journal Socience: 266, 690–703.

Williamson, B. J., Spratt, J., Adams, J. T., Stanley, C. J. 2000. Geochemical constraints from zoned hydrothermal tourmalines on fluid evolution and Sn mineralization: an example from on Fault Breccias at Roche, SW England. Journal of Petrology: 41, 1439–1453.